PAPER • **OPEN ACCESS**

Engineered albumin hydrogel with *in-situ* silver oxide nanoparticles for biomedical applications

To cite this article: Smrity Sonbhadra *et al* 2025 *Nano Ex.* **6** 025005

NANO EXPRESS

PAPER

Engineered albumin hydrogel with *in-situ* silver oxide nanoparticles for biomedical applications

Smrity Sonbhadra[1,4], **Rushikesh Fopase**[1,4], **Anurag Mishra**[2], **Nandini Dhakaan**[3] and **Lalit M Pandey**[1]

[1] Bio-Interface & Environmental Engineering Lab, Department of Biosciences and Bioengineering, Indian Institute of Technology Guwahati, Guwahati, Assam, India
[2] Centre for the Environment, Indian Institute of Technology Guwahati, Guwahati, Assam, India
[3] School of Biomedical Engineering, Indian Institute of Technology (BHU) Varanasi, Varanasi, Uttar Pradesh, India
[4] Equal contribution.

E-mail: lalitpandey@iitg.ac.in

Keywords: hydrogels, antibacterial, mechanical strength, biomedical

Supplementary material for this article is available online

OPEN ACCESS

RECEIVED
22 February 2025

REVISED
7 April 2025

ACCEPTED FOR PUBLICATION
10 April 2025

PUBLISHED
23 April 2025

Abstract

Hydrogel-based treatment strategies have proven their significance in the field of drug delivery, wound healing, and tissue scaffolds, offering significant advantages over conventional treatment methods. The present study attempts to assess the hydrogel formation capability of a biopolymer, bovine serum albumin (BSA), without the addition of any crosslinker agents. Next, the *in situ* synthesis of silver (Ag) nanoparticles into the hydrogel was explored at two different concentrations of Ag as BSA + 5 mM AgNPs (BSA5) and BSA + 10 mM AgNPs (BSA10). The thermally aggregated BSA+Ag hydrogels exhibited excellent gel consistency with the successful formation of Ag nanoparticles. The incorporation of Ag nanoparticles (AgNPs) into the BSA hydrogel matrix was confirmed via the peaks obtained through Fourier Transform Infrared Spectroscopy (FTIR) and x-ray diffraction (XRD) analysis. In FTIR, prominent redshifts (when compared with control BSA without Ag incorporation) suggested the interaction of peptide bonds of BSA with the surface of AgNPs, whereas the XRD analysis showed the presence of AgNPs in two distinct phases, i.e., Ag_2O and AgO. Field emission scanning electron microscopy (FESEM) revealed random distribution and irregular shapes of the synthesized AgNPs, with an average size of particles being 67 ± 20 nm and 62 ± 21 nm in BSA5 and BSA10, respectively. Moreover, the integration of AgNPs within the BSA hydrogel matrix tuned the hydrophobicity, swelling ratio, and rheological properties. The hydrogel became hydrophobic in the presence of nanoparticles, which, in turn, reduced the swelling ratio. The nanoparticles significantly enhanced the critical stress threshold for the hydrogel from 6.2 Pa to 175 Pa. Antibacterial tests confirmed the broad-spectrum activity against pathogenic gram-positive and gram-negative bacteria in a dose-dependent manner. The cytotoxicity analysis of the synthesized BSA+Ag hydrogel exhibited over 90% cell viability, highlighting excellent biocompatibility. With effective antibacterial properties and low toxicity, the prepared BSA + Ag hydrogels highlighted their suitability for future biomedical applications.

1. Introduction

Biomaterials have been a central theme in biomedical sciences for the past few decades. The emergence of engineered biomaterials has transformed medical treatments by enabling targeted drug delivery, promoting tissue regeneration, and advancing diagnostics through biosensors. Hydrogels, in particular, have become ideal materials owing to their excellent biocompatibility and tuneable physical, chemical, and mechanical properties [1]. The structure is formed by crosslinked polymer chains held together by covalent bonds, ionic interactions,

or hydrogen bonds. This network creates a highly porous architecture, allowing the diffusion of molecules and fluids and making them widely suitable for biomedical applications [2]. The three-dimensional structure of hydrogels absorbs and retains large amounts of water and encapsulates bioactive agents.

Many materials, both synthetic including, polyvinyl alcohol (PVA), polyacrylic acid (PAA), and polyacrylamide (PAAm) and naturally occurring including, gelatine, fibrin, chitosan, alginate, and serum albumin, have been explored as hydrogels. Albumin is widely used as a raw material for hydrogel preparation due to its abundance of amino acid residues [3]. Albumin comprises 583 amino acid residues, including 34 cysteines, 17 disulfide bonds, a free sulfhydryl group at position 34 of the peptide chain, and various functional groups like amino and carboxyl groups. Serum albumin, a naturally occurring, non-glycosylated protein with a molecular weight of 66.4 kDa, constitutes approximately 60% of the total protein content in blood [4]. It is a readily available, sustainable, biocompatible, and potentially autologous biomaterial with diverse clinical and biomedical applications. These features allow the formation of albumin hydrogel networks and can be crosslinked with other materials [3]. In this direction, serum albumin would be the focus of interest for this paper.

The biological performance of hydrogels is regulated by rheological properties, which can be tuned by the degree of crosslinking and additives. The degree of crosslinking determines the flexibility, swelling, and mechanical stability required. On the other hand, additives such as nanomaterials reinforce the hydrogel by balancing the stiffness and the elasticity as per the requirements. Along with this, the nanomaterials also add in their innate characteristics; for example, Ag and Au nanoparticles (NPs) offer antibacterial activity [5], while Fe_3O_4 nanomaterial adds magnetic features to the hydrogels [6, 7]. In a study by Markus *et al* it was highlighted the strong antimicrobial properties of chitosan-based hydrogels containing AgNPs, effectively targeting a range of pathogens, including methicillin-resistant *Staphylococcus aureus* (MRSA) and *Candida albicans* [8]. de Camargo *et al* reported that alginate-based hydrogels embedded with gold NPs exhibited potent antifungal activity against *Aspergillus fumigatus* [9]. Another study reported the antibacterial properties of titanium dioxide NPs incorporated into a hydrogel system to inhibit bacterial growth [10]. Further, the implementation of an *in situ* synthesis approach for the nanomaterials incorporated in hydrogels offers better dispersion, stability, improved interfacial interactions, reduced reaction time, and spent or byproducts.

In this regard, the present study explores the scope of the bovine serum albumin (BSA) hydrogel for antibacterial features by a facile *in situ* synthesis of AgNPs. Two concentrations of Ag precursor (silver nitrate ($AgNO_3$)), 5 and 10 mM, were employed during the synthesis to avoid the possible concentration-dependent toxic effects of the Ag nanoparticles. The selection of the concentrations of Ag precursor was based on the inferences made by a previous study [11]. The prepared AgNPs incorporated hydrogel and were characterized for wettability, swelling properties, and rheological aspects. The antibacterial potential of the prepared AgNPs incorporated BSA hydrogel was assessed against the clinically relevant pathogenic bacterial strains, including gram-positive and gram-negative bacteria. The cytocompatibility studies were performed to evaluate the suitability of prepared hydrogels for biological applications.

Interestingly, the hydrogel has the ability to trap and retain molecules, which provides an innovative way for drug delivery, one of which is through nanoparticle-hydrogel systems. This synergistic system frames a new class of biomaterials that are designed to integrate the beneficial characteristics of the individual materials, i.e., hydrogels and nanoparticles (NPs) for drug delivery, wound healing, and other applications [12]. In recent years, efforts have been made to synthesize biocompatible materials with a broad spectrum of antibacterial properties for topical applications using nanoparticle-hydrogel systems. Ongoing research in this field suggests that the free space within the 3D network structure of hydrogels can store NPs, enabling controlled release for targeted drug delivery. These systems offer several advantages, like enhanced drug solubility, improved drug localizations and bioavailability for controlled release of therapeutic agents, protection of drug molecules from degradation by biological fluids, reduction in dosage, and minimizing the side effects of the drug [13]. A key advantage of NP-integrated hydrogels is their adaptability for delivering various antimicrobial agents. For example, antibiotics like amoxicillin and cephalexin can be embedded within hydrogels to enable targeted delivery to infection sites [14]. Recent studies have emphasized the potential of NP-infused hydrogels as a treatment for various infections, including those caused by bacteria and fungi [13, 15]. Silver (Ag) metals integrated into nanomaterial systems have gained significant attention in recent years. AgNPs possess unique properties, including catalytic and antibacterial activities. Despite the benefits of AgNPs, one major concern is the toxicity of NPs for humans and environmental health, given that their size, which can be considered their main advantage, also contributes to their ability to cross barriers in organisms, causing mild to chronic toxic effects after their accumulation. Hence, the toxic effects of AgNPs should also be taken into consideration during their synthesis and application.

Although AgNPs and hydrogels have been extensively studied, there is significant potential for research to evaluate the antibacterial activity when incorporated into topical applications. Therefore, in this study, the benefits of both hydrogels and AgNPs have been combined to be used for biomedical applications. Bovine serum albumin (BSA) hydrogel has been prepared without the addition of any crosslinker agents. Further, AgNPs were

synthesized *in situ*, followed by the analysis of the physical, chemical, and biological properties of the engineered hydrogels. Morphology, phase analysis, and function groups of the synthesized AgNPs incorporated into BSA hydrogels were analyzed. Then, the wettability, rheological, and swelling properties of the prepared hydrogels were studied. Further, antibacterial and cytocompatibility analyses of synthesized hydrogels were performed.

2. Materials and methods

In the study, BSA (MB083), silver nitrate ($AgNO_3$) (PCT1307), and Luria Broth (LB) (G575) were procured from Himedia, while sodium borohydride ($NaBH_4$) was obtained from Spectrochem (011925). Milli-Q (MQ) water with a resistance of 18.9 MΩ cm^{-1} was used for all experiments to ensure high purity and consistency.

2.1. Synthesis of BSA-Ag hydrogels

Ag-conjugated BSA hydrogels were prepared following a facile *in situ* formation process [16]. Briefly, 10% BSA in 5 ml of NaCl buffer (pH 9.0) was added to petri plates and incubated at 70 °C for 5 h to get a hydrogel-like texture. The heat-induced aggregation of the BSA provides a matrix that forms a hydrogel network. For the *in situ* synthesis of AgNPs, 5 and 10 mM $AgNO_3$ solutions were mixed with 10% BSA in NaCl buffer at room temperature. 0.2 ml of 100 mM $NaBH_4$ was added dropwise to the mixture, resulting in the formation of a brown color. NaBH 4 acts as a strong reducing agent, reducing Ag^+ ions to their elemental form (Ag°), which leads to the formation of AgNPs. The solutions were stirred for 10–15 min to ensure thorough mixing. Subsequently, the mixtures were transferred to Petri plates and incubated at 70 °C for 5 h to get a hydrogel-like texture. The BSA matrix helps encapsulate and stabilize AgNPs, enabling their uniform spreading in the gel matrix. Three sample variants were prepared: BSA, BSA + 5 mM AgNPs (BSA5), and BSA + 10 mM AgNPs (BSA10).

2.2. Characterization studies of synthesized hydrogels

The prepared hydrogel samples were visually analyzed for the gel-like feature and the effects of AgNPs incorporation. The synthesized hydrogels were further characterized using various techniques, including Field emission scanning electron microscopy (FESEM), Energy Dispersive x-ray Spectroscopy (EDX), Fourier Transform Infrared Spectroscopy (FTIR), x-ray diffraction analysis (XRD), mechanical strength determination using rheological studies, wettability analysis using contact angle measurement, and swelling index studies.

2.2.1. FESEM and EDX of synthesized hydrogels

FESEM was performed to characterize the morphology of the synthesized AgNPs [17]. The AgNPs embedded in the hydrogel substratum were completely dried at a moderately high temperature (50 °C) to avoid any distortion in NP structures. A fine section (0.5 cm × 0.5 cm) dimension from the synthesized hydrogels incorporated with AgNPs was taken to visualize the morphological details. The surfaces were then coated with gold sputtering and examined using FESEM (FESEM, Zeiss, Model: Sigma). The obtained size (length of the NPs) was calculated using ImageJ software, and the resultant size distribution of the particles was determined to estimate the average size of the NPs [18].

To determine the elemental composition of the synthesized hydrogels and confirm the silver doping, EDX (Zeiss, Model: Sigma) analysis was performed. The samples were dried to avoid any charging due to possible moisture and placed on a carbon-coated copper grid followed by a gold coating via sputtering. Quantitative elemental analysis was found through the atomic and weight percentages of different elements present in the sample [19].

2.2.2. FTIR and XRD analysis of synthesized hydrogels

The synthesized hydrogel, comprising various combinations (BSA, BSA5, and BSA10), was characterized and compared using FTIR Spectroscopy (Perkin–Elmer, Spectrum Two). This technique identifies the functional (chemical) groups within the sample compound. Infrared radiation induces molecular vibrations (stretching or bending) and rotations at specific frequencies corresponding to the compound. A detector records these interactions as peak intensities at particular wavelengths [16]. The intensity and characteristic vibration of each peak indicate the functional groups associated with the sample's chemical structure. Specifically, ∼1 mg of the synthesized hydrogel was analyzed in the mid-infrared range (400–4000 cm^{-1}) using an FTIR spectrophotometer, with room moisture content controlled. The spectral resolution was set at 4 cm^{-1}, with a scan rate of 40 scans [20]. An analysis was conducted on hydrogel powders using a Rigaku Smartlab, a 9 kW x-ray diffraction apparatus from Japan. The x-ray source utilized Cu-Kα radiation, with a test voltage of 125 kV and a current of 40 mA. The diffraction pattern of blank BSA samples, BSA5 and BSA10, were investigated over the range of 10° to 90°. The standard International Centre for Diffraction Data (ICDD) files were utilized to verify

the different phases acquired and assess the alterations in the lattice characteristics. The sizes of the crystallites were calculated using the Debye–Scherrer formula, as described in equation (1).

$$D = \frac{k\lambda}{\beta \cos\theta} \tag{1}$$

Here, k represents Scherer's constant (0.94), λ represents the wavelength of x-ray (1.54 Å), θ represents Bragg's angle, and the Full width at half maximum (FWHM) of the diffraction peak is β [21].

2.2.3. Wettability, rheological, and swelling properties of the synthesized AgNPs

The contact angle (C A) of water was measured at the surface of BSA, BSA 5, and BSA10 hydrogel using a Goniometer and drop shape analysis system (Holmarc, India). A water sample of 2 μl was dropped onto each surface, and the C A. value was determined by analyzing the picture of the drop shape [22]. The rheological properties of the synthesized hydrogels were measured using a rotary rheometer (MCR72, Anton Paar) with the parallel plate geometry. The hydrogels were added between the two parallel plates with 1 mm clearance. The storage modulus (G′) and loss modulus (G″) were reordered [23].

The gravimetric method was used to examine the composite hydrogel's swelling index. The samples were freeze-dried, and the initial weight (W_i) was determined. After that, the Samples were immersed in the PBS and SBF buffer (pH 7.4) at 37 °C. After a fixed time interval, the samples were removed from the buffer solution. The surplus PBS and SBF solution on the sample's surface was removed using filter paper. Again, the weight of the wet samples was recorded as *Wf*. The swelling rate for each sample at each time interval was determined using equation (2) below [24]. Each experiment was repeated three times.

$$S_R(\%) = \frac{W_f - W_i}{W_i} \times 100 \tag{2}$$

2.3. Determining antibacterial and cytocompatibility analysis of synthesized hydrogels

The antibacterial properties of synthesized BSA-Ag hydrogels were assessed using the agar well-diffusion method [25]. Wells were created on MHA agar plates, where the hydrogel samples were loaded. To facilitate diffusion, 10% NaOH was added above the hydrogels. Pathogenic bacterial strains, *S. aureus* (gram-positive) and *Escherichia coli* (gram-negative), were cultured overnight in LB media and then spread aseptically over the agar surface. The plates were incubated at 37 °C for 24 h in a shaker incubator. The effectiveness of the hydrogels was determined by the formation of clear inhibition zones around the wells, indicating antibacterial activity [26]. BSA served as the negative control, while kanamycin was used as the positive control. The appearance of inhibition zones around the hydrogel samples demonstrated their antibacterial efficacy against both *S. aureus* and *E. coli*.

Further, the cytocompatibility of the prepared hydrogels was assessed using the MTT assay (3-(4,5-dimethylthiazol-2-yl)-2,5-diphenyltetrazolium bromide) according to the standard guidance by ISO-10993-5 [27]. HEK-293 cells were used as a model cell line for the experiments. The cells were cultured in the CO_2 incubator (Galaxy 170S, Eppendorf) using Dulbecco's modified eagle medium (DMEM) supplemented with 10% fetal bovine serum and 1% antibiotic solution. For the experiment, 10^4 cells were seeded to the wells and added with an equal amount of respective hydrogels of different compositions. Prior to experiments, the hydrogels were overnight dipped in the DMEM media. After the incubation period, 48 and 96 h, 100 μl of MTT solution in DMEM was added to wells, followed by 4 h of incubation. The resultant formazan crystals were dissolved in the dimethyl sulfoxide, and the absorbance was recorded at 570 nm using a multiplate spectrophotometer (FLUOstar Omega, BMG Labtech). The cell viability was determined using the formula.

$$Cell\ Viability = \frac{Absorbance\ of\ Sample_{570\ nm}}{Absorbance\ of\ Control_{570\ nm}} \tag{3}$$

2.4. Statistical analysis

The data obtained for each experiment was analyzed using OriginPro 8.5, which was used to perform the statistical analysis. All experiments were performed in triplicates, and the values were reported by measuring the average ± standard deviation.

3. Results and discussions

3.1. Synthesis and morphological and elemental analysis of hydrogels

Three different types of hydrogels were synthesized by following the procedure mentioned in section 2.1, as shown in figures 1(A)–(C). All three hydrogels exhibited gel-like consistency and visually distinguishable

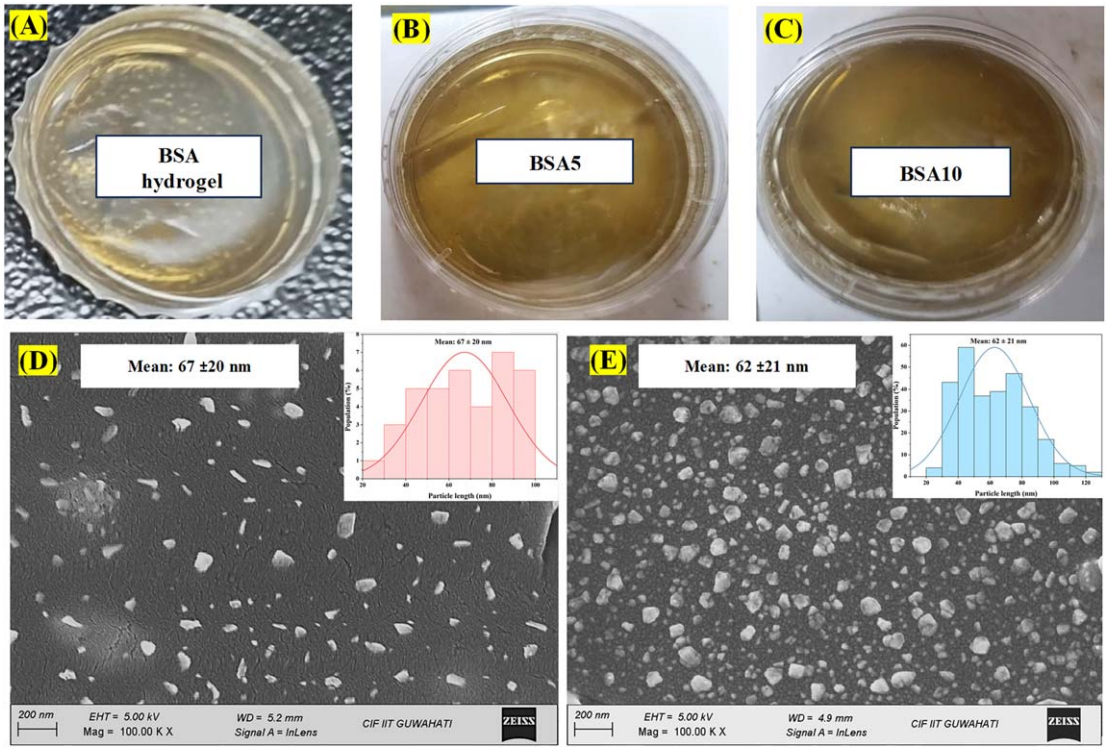

Figure 1. Synthesized Ag-conjugated BSA hydrogels; (A) BSA , (B) BSA5, and (C) BSA10 and FESEM micrographs of synthesized hydrogels; (D) BSA5, and (E) BSA10.

appearance. BSA-only hydrogel showed an opaque or semi-translucent appearance. In contrast, the BSA5 and BSA10 hydrogels showed reduced translucency with an increasing brownish appearance, indicating the presence of AgNPs formed due to the addition of a reducing agent ($NaBH_4$) during the synthesis process [28, 29].

The FESEM images revealed the structural details of the synthesized AgNPs. The NPs were found to be of irregular shape and randomly distributed, with a major resemblance to that of squares (and a few spherical), as shown in figures 1(D) and (E). The AgNPs in BSA5 were comparatively less densely populated than that of BSA10, corresponding to the proportion of AgNP concentrations. The average sizes of the AgNPs in BSA5 and BSA10 hydrogels were found to be 67 ± 20 nm, and 62 ± 21 nm, which is in accordance with the size of NPs reported in the literature [16, 17].

The EDX analysis of the BSA5 and BSA10 hydrogels revealed the presence of carbon (C), nitrogen (N), oxygen (O), and silver (Ag) as constituent elements, as shown in figure 2. The elements like C, N, and O corresponded to the peptide bonds from the BSA protein, and the presence of Ag confirmed the facile *in situ* addition of AgNPs, found in accordance with the literature [18, 28]. Figure 2(A) showed the presence of peptide bonds of BSA-only hydrogel (without Ag doping) with the highest relative atomic abundance of C (49%), followed by O (33%) and N (17%). Further, a similar sequence of elements' abundance of C, followed by O and N, corresponded to the peptide (organic) nature of the sample in both BSA5 and BSA10 hydrogels, as BSA protein was provided as the base matrix [30]. Moreover, figure 2(B) showed an atomic distribution of Ag at about 1.8%, corresponding to BSA5. Similarly, figure 2(C) confirmed a higher proportion of Ag corresponding to BSA10 (nearly double with BSA5), i.e., about 2.5% of atomic distribution, which aligned with the designed experimental hypothesis. A few random peaks were also observed in all three graphical spectra, indicating some signal noise, Au coating during sample preparation for EDX, and a few others for some of the salts used during the hydrogel synthesis procedure.

3.2. Characterization of synthesized hydrogels

3.2.1. FTIR and XRD analysis of synthesized hydrogels

The FTIR spectra of BSA and BSA with AgNP samples (BSA5 and BSA10) were obtained, as shown in figure 3(A). All three prepared hydrogel samples exhibited the major peaks corresponding to the interaction in the protein structure. The significant peak in the 1620–1640 cm−1 1620–1640 cm^{-1} range corresponds to the amide I band within the protein structure (C=O stretching of α-helix and β-pleated sheets). The peak around 1530–1540 cm^{-1} corresponded to amide II bands of BSA protein, and the distinct peak near 1450 cm^{-1} corresponded to amide III bands (showing C-N stretching and N-H bending). Meanwhile, peaks in the range 3280–3290 cm^{-1} corresponded

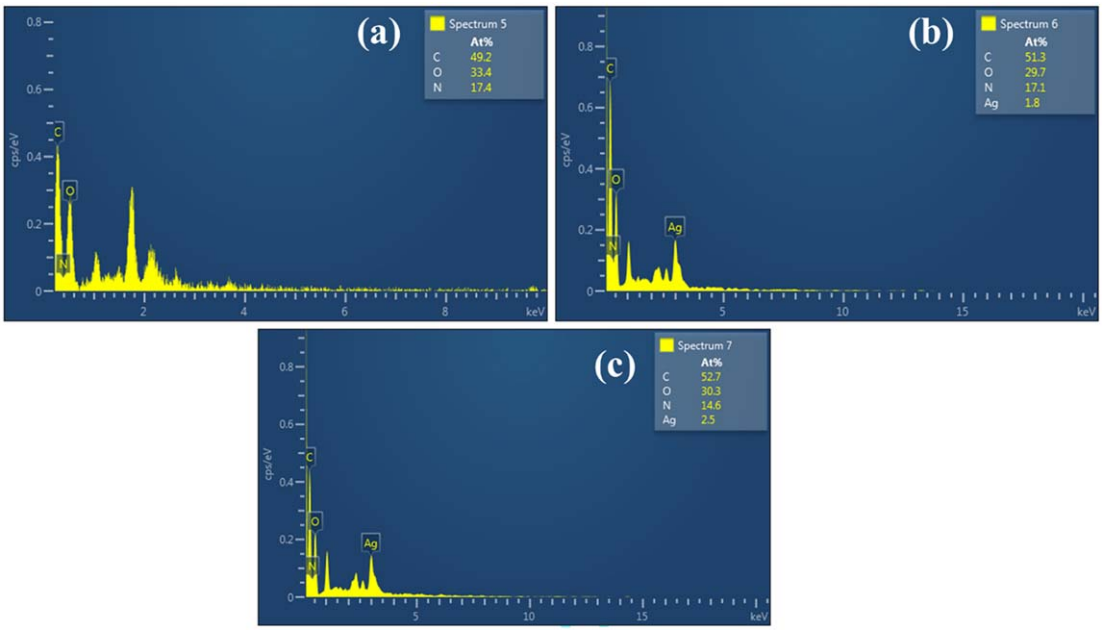

Figure 2. Elemental analysis of synthesized BSA-Ag hydrogels (a) BSA (blank), (b) BSA5, and (c) BSA10 depicting the major elements present in the samples.

to the amide A band (mainly representing the N-H Stretching) [22, 29]. Comparing the control sample of BSA hydrogel with its counterparts of AgNPs incorporated samples, the vibrations (particularly in amide bands) at 3294, 1640, 1542, 1453, and 1392 cm^{-1} in BSA exhibited the redshifts to 3286, 1638, 1541, 1450, and 1389 cm^{-1} in BSA5, and to 3281, 1636, 1538, 1446, and 1387 cm^{-1} in BSA10, clearly indicating influence of Ag presence, that was in accordance with the fact as reported in the literature [30, 31]. The shifting can be understood due to the coordination or binding of the above-mentioned functional groups to the surface of AgNPs at different wavenumbers [32]. The higher the Ag concentration, the more prominent the shift, suggesting that the peptide bonds of BSA are interacting with the surface of AgNPs [33, 34]. The other vibration bands of these three samples remained almost unchanged, which is attributed to the peaks corresponding to the stretching and bending of peptide bonds (N-H and C=O) and the amide region (-CO-NH-) [33].

The effects of hydrogel formation and AgNP interactions on the secondary structures of BSA were analyzed through the variation in the amide I region observed from the deconvolution of the FTIR spectra (figure 3(B)). The deconvoluted amide I region between the wavenumber 1700–1600 cm^{-1} highlighted the change in the secondary structure of the BSA (figure S1). As reported, the native BSA contains ~66% α-helix, 22% β-sheets, and 13% turns [35]. The gel formation process, i.e., heat-induced aggregation, involves the formation of β-sheets content at the cost of α-helix. Such transition occurs through intramolecular hydrogen bonds forming, leading to a 3-dimensional gel-like structure [36]. The high temperature partially unfolded the BSA structure due to hydrogen bond breaking, with reducing α-helix and increasing β-sheets contents. During the process, the exposed hydrophobic region of BSA, newly formed hydrogen bonds, and the resultant electrostatic interaction leads to the formation of the hydrogel of the BSA structure [3]. For the present hydrogel samples, the observed changes in the secondary structure of the BSA are given in table S1. The BSA-only hydrogel showed the α-helix (1655.47 cm^{-1}) and β-sheets (1625.20 and 1690.86 cm^{-1}) contributions of 24.48% and 29.30%. The reduction in the α-helices content can be justified by the presence of other secondary structures like random coils (23.07%), β-turns (12.17%), and side chains (10.97%). Similar heat-induced changes in α-helices and β-sheets were reported by previous studies [37]. There were no significant effects on the secondary structure due to the incorporation of 5 mM of AgNPs in the BSA hydrogels. The amide I region for BSA0 and BSA5 showed similar patterns (figure 4(B)). Further, the 10 mM AgNPs addition in the hydrogel increased β-sheets content to 35.58% along with the random coils (26.53%). The α-helix content was decreased to 22.34% with the other secondary structures, β-turns (6.56%), and side chains (9.00%). The increase in random coils is probably due to the increased disruption of hydrogen bonds and the resultant electrostatic interactions occurring during the hydrogel formation. Moreover, the tendency of metal–protein coordination via amino acids also hinders the folding patterns of β-sheets, resulting in increased random coils.

An XRD analysis was used to confirm the formation of AgNPs and their interactions with BSA, as shown in figure 3(C). The BSA hydrogel showed a broad peak near the *2-theta* position of 22.52° corresponding to the

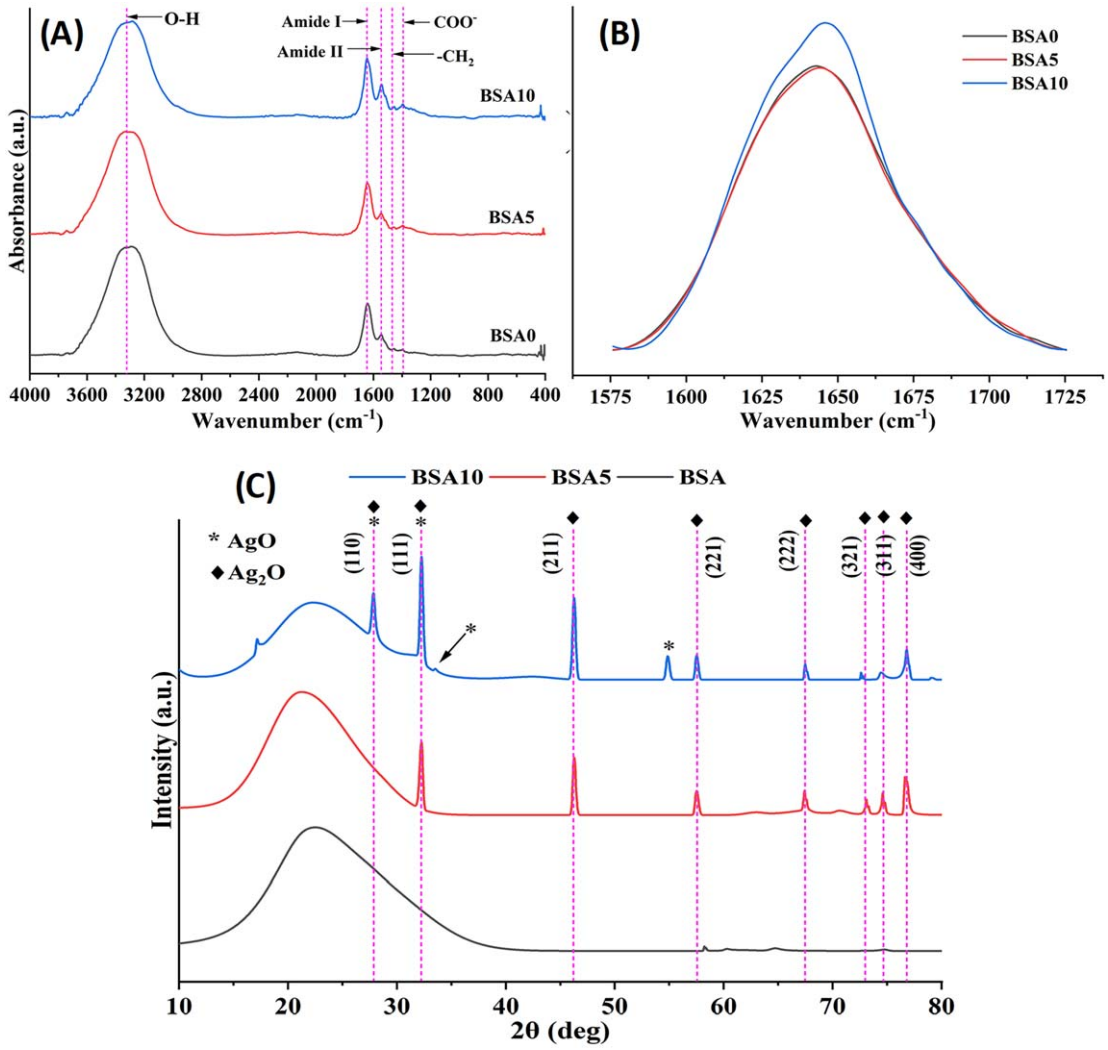

Figure 3. (A) Complete FTIR spectra, (B) amide I region of FTIR spectra, and (C) XRD analysis of synthesized hydrogels, only BSA, BSA5, and BSA10, respectively.

amorphous or partially crystalline nature of the protein. Such a peak arises due to the intermolecular hydrogen bonding interactions between protein chains [38]. The BSA hydrogel incorporated with 5 and 10 mM Ag exhibited peaks at the *2-theta* positions of 27.95° (100), 32.26° (111), 46.28° (211), 57.28° (221), 67.5° (222), 73.06° (321), 74.07° (311) and 76.86° (400) corresponding to the cubic Ag_2O (ICDD No.: 01-076-1393, 01-078-5868) highlighting the crystallinity of nanoparticles [39]. While, some extra peak appeared at 33.51° and 54.82° corresponding to AgO phase (ICDD No.: 01-076-1489) along with overlapping peak positions at the *2-theta* of 27.82° and 32.27°. The crystallite sizes calculated for formed AgNPs for 5− and 10 mM Ag samples using Debye–Scherrer's formula were 26.71 and 30.14 nm, respectively. The observed diffraction patterns confirmed the presence of AgNPs in BSA hydrogels. XRD patterns indicated the formation of AgNPs with possible contributions from oxidized silver phases (Ag_2O and AgO), suggesting partial surface oxidation during synthesis. It can be hypothesized that the reduction of Ag^+ ions resulted in the formation of Ag^0, which subsequently underwent oxidation in the hydrogel environment to form Ag_2O. However, at the higher concentration of 10 mM, $NaBH_4$ was unable to completely reduce all the Ag+ ions to Ag^0. The remaining ions are likely to facilitate redox interaction with Ag_2O to yield the AgO phase, evident in the XRD peaks. Therefore, only BSA10 have shown peaks for AgO in the diffraction pattern. The presence of AgO is expected to enhance the antibacterial properties due to higher oxidation potential, as discussed later.

3.2.2. Swelling, wettability, and rheological behavior of the synthesized hydrogels

The swelling property indicates the medium uptake ability of composite hydrogels under physiological conditions. However, an overabundance of swelling can impact the structural stability of the hydrogel, leading to increased pressure on the surrounding tissue. The lack of clinical applicability results from inadequate properties, whereas incorporating suitable swelling properties enhances the adaptability of composite hydrogels

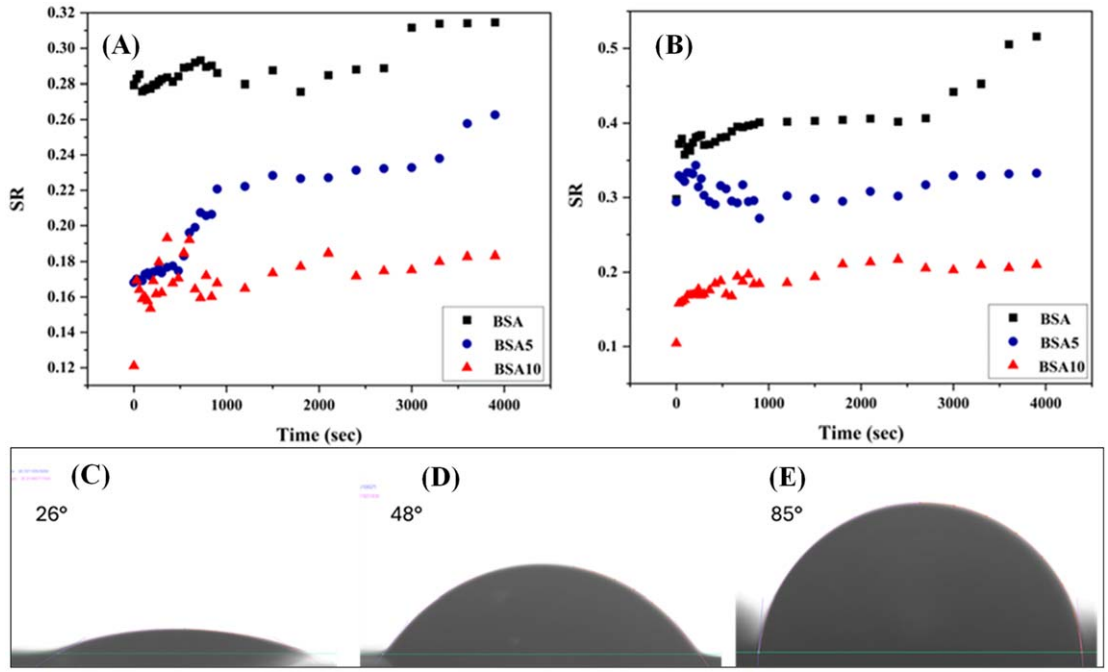

Figure 4. Swelling rate in (A) PBS) and (B) SBF and water contact angles of (C) BSA, (D) BSA5 and (E) BSA10 hydrogels.

to physiological conditions. The swelling behavior of BSA/AgNPs composite hydrogel in PBS and SBF buffer is shown in figures 4(A) and (B). The swelling indices measurement of the BSA, BSA5, and BSA10 hydrogel samples in the SBF showed a decreasing order of BSA10 < BSA5 < BSA. The lower swelling index value is related to the positive attributes of AgNPs, precisely their effective barrier properties and hydrophilicity [7]. In a study, a similar phenomenon was observed where scaffolds that were modified with higher concentrations of TiO_2 nanoparticles exhibited reduced swelling behaviour [38]. The inclusion of AgNPs in the BSA hydrogels resulted in a reduction of the electrostatic force. As the AgNPs+ BSA hydrogel swells in the PBS and SBF solution, the silver ions (Ag^{+}) stabilize within the hydrogel pores. The metal ions are attached to the functional groups of hydrogel networks, specifically the alcohol '-OH' and carboxylic groups '-COO-.' Hence, significant quantities of silver ions can be effectively captured within the cavities of the hydrogel networks [39]. In addition, the observed swelling degree could be linked to the absorption process that controls the diffusion of water molecules and other hydrophilic substances, like salts, into the pores of the hydrogel network.

Next, the water wettability measurements for the BSA, BSA5, and BSA10 hydrogel showed contact angles of $26.73° \pm 0.5$, $58.11° \pm 1.19$, and $85.39° \pm 0.76$, respectively, as shown in figure 4. The results indicate that hydrophobic interactions likely play a significant role in the binding of BSA to AgNPs. This interaction is influenced by both enthalpy and entropy of the interaction mechanism between carbonyl groups (C=O bonds of α-helix and β-sheets). A study on BSA and AgNP interactions reported a positive enthalpy change ($\Delta H°$), indicating energy associated with intermolecular bond formation, and a positive entropy change ($\Delta S°$), suggesting an entropy-driven and endothermic process primarily governed by hydrophobic forces [40]. Similarly, in the present study, the temperature (65 °C) contributed to the enthalpy-driven hydrogen bondings, which further led to entropy-driven hydrophobic interactions due to the release of bound water molecules. The increased hydrophobicity of the BSA-Ag hydrogel can be understood due to the exposure of more β-sheets (because of protein unfolding) and a reduction in the overall α-helix content in the BSA. Such alterations resulted in the observed increment of the surface contact angles for the BSA-based hydrogels [41]. The effect of binding of the Ag ions with the BSA matrix was also confirmed by the FTIR spectra, indicated through the observed redshifts. The hydrophobic nature of BSA10 hydrogel also corresponded to the least value swelling ratio (figure 4). Hydrophobicity and swelling ratio are inversely correlated [42]. The observed wettability properties enable the medical application of a synthesized hydrogel (BSA-AgNPs) by enhancing its safety and effectiveness. In addition, as the concentration of AgNP increases and a protein corona structure forms, it is likely that the cytotoxicity of the NPs and their interaction with cell membranes are diminished [43].

The rheological properties of a hydrogel composed of BSA, BSA5, and BSA10 using a rheometer equipped with a parallel plate geometry. The amplitude and stress sweep tests were conducted to examine hydrogel behavior with varying shear strain and stress, respectively, as shown in figure 5. The strain dependence of G′ and G″ can be observed from the pattern. An amplitude sweep test was initially conducted on BSA, BSA5, and BSA10

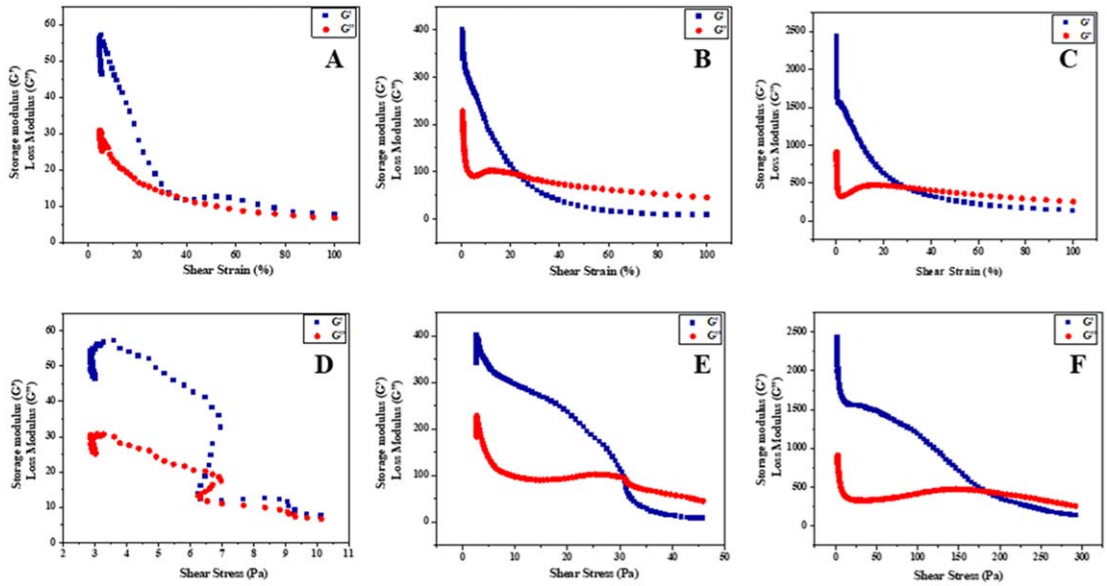

Figure 5. Results of the Amplitude-sweep measurements performed at room temperature on the (A) BSA hydrogel, (B) BSA5, and (C) BSA10. Results of the Stress-sweep measurements performed at room temperature on the (D) BSA hydrogel, (E) BSA5, and (F) BSA10.

hydrogel. The results indicate that at low shear strain, G′ was significantly greater than G″, suggesting a predominance of elastic behavior. In the case of BSA hydrogel, initially, G′ was approximately 50 Pa, which was increased by adding 5 mM AgNPs and 10 mM AgNPs in BSA hydrogel to 342 Pa and 1989 Pa, respectively. As shear strain increased, G′ started to decline and reached a critical strain point, where G″ started growing, demonstrating the transition from solid to liquid phase. A comparable observation occurred upon the addition of AgNPs to the hydrogel. The storage modulus increased with the addition of AgNPs due to the predominance of hydrophobic forces associated with their incorporation [23]. Also, the increased β-sheet content in the hydrogel samples enhances the rigidity within the hydrogel due to the intermolecular hydrogen bonding, leading to a significant decrease in the shear stain.

The stress sweep test was also performed for BSA, BSA5, and BSA10 hydrogel. The BSA hydrogel G′ and G″ was stable at low shear stress when G′ reached the critical stress threshold at the value of shear stress 6.2 Pa; after that, a decrement was observed in the value of G′s, while the value G″ showed a pronounced increase, which represents the transition of elastic behavior to viscous behaviour [43]. However, incorporating AgNPs elevates the critical stress threshold for BSA5 and BSA10, measured at 30 Pa and 175 Pa, respectively, as illustrated in figure 5. The results indicated that the incorporation of AgNPs enhances the critical stress threshold value, demonstrating an increased elastic strength of the hydrogel. The results indicate that AgNPs play a significant role in forming the crosslinked BSA. The observed increase in elastic modulus relative to the control gel can be attributed to the additional crosslinking facilitated by the surface-enhanced AgNPs [44, 45]. The increased intermolecular hydrogen bonding in the β-sheets increases the crosslinking network and thus further helps to increase the shear stress of the hydrogels.

3.3. Antibacterial and cytocompatibility assessment of synthesized hydrogels

The synthesized BSA-conjugated Ag hydrogels demonstrated significant antibacterial activity against both gram-positive (*S. aureus*) and gram-negative (*E. coli*) pathogenic bacteria. Figure S2 shows the antimicrobial effect of BSA-Ag NPs through the observed zone of inhibition (ZOI) (reflected as diameter in cm) for the pathogenic bacterial strains. Kanamycin was used as positive control at their minimum inhibitory concentrations of (MIC) value of 50 $\mu g\,ml^{-1}$. The results suggested that the prepared hydrogel was more effective against gram-positive (*S. aureus*), showing a ZOI of 1.1 ± 0.2 cm for BSA5 and 2.1 ± 0.3 for BSA10, which is comparable with the ZOI value produced by the positive control 2.5 ± 0.5 cm. Whereas, against gram-negative (*E. coli*), the ZOI obtained was 0.6 ± 0.1 cm with BSA5 and 1.3 ± 0.2 cm with BSA10, which aligns with the positive control ZOI value of 1.8 ± 0.4 cm. A higher susceptibility of gram-positive bacteria against antibiotic agents in comparison to gram-negative bacteria was found due to the differences they possess in their cell wall structure (lacks an external lipopolysaccharide membrane which allows an easy target of antibiotic agents to disrupt the cell), cell physiology, and respective metabolism, as reported elsewhere [44, 45]. The statistical significance for the three different groups (positive control, BSA5, and BSA10) was calculated using one-way ANOVA with a post-hoc Tukey HSD Test, as represented by the p-values in figure 6(A). These findings suggest

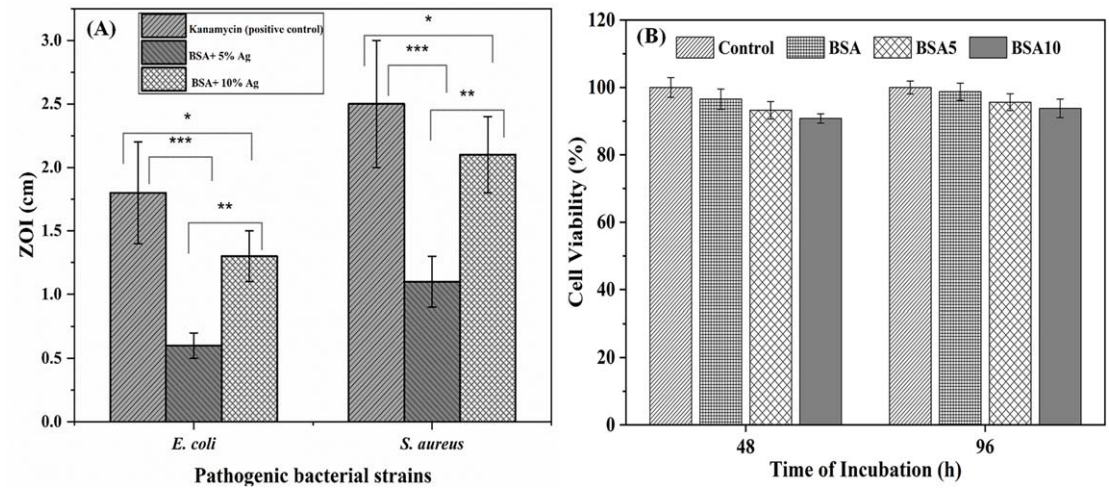

Figure 6. (A) The zone of inhibition measured as diameter (in cm) formed by the antibacterial property reflecting agents of the synthesized hydrogels against *E. coli* (gram-negative) and *S. aureus* (gram-positive) (* *p*-value > 0.5 (0.659), ** *p*-value < 0.5 (0.317), and *** *p*-value $<< 0.15$ (0.141) and (B) Cytocompatibility assessment of the BSA and BSA-Ag hydrogels against the HEK-293 cells for the incubation of 48 and 96 h.

that BSA-conjugated Ag hydrogels have comparable antibacterial efficacy with antibiotics like kanamycin against broad-spectrum bacterial groups. Further, the finding of the present study exhibiting the antibacterial efficacy of AgNPs against pathogenic strains aligns with other similar studies reported in the literature. For instance, in a study, the modified AgNPs showed a strong antibacterial effect against *E. coli* and *S. aureus*, with the minimum inhibitory concentration (MIC) found as 0.84 and 1.69 $\mu g\,ml^{-1}$ Ag, respectively, confirmed through the disk diffusion method [46]. In another study, the synthesized AgNPs demonstrated a concentration-dependent antibacterial action, giving a 100% killing of *E. coli* (gram-negative) and *P. aeruginosa* (gram-positive) cells at the AgNPs concentrations of 4.5 and 2.7 $\mu g\,ml^{-1}$, respectively, measured through spread-plate method [47]. Likewise, in a different study, the antibacterial efficacy of AgNPs was determined against *P. aeruginosa* through the well-diffusion method, for which the MIC value was found to be 2 $\mu g\,ml^{-1}$, and a linear trend was observed for increasing ZOI with increasing AgNP concentration (1–5 $\mu g\,ml^{-1}$) [48]. Moreover, the impact of Ag metal (present in its two major forms i.e., AgO and Ag_2O in the synthesized hydrogel) can also be interpreted in terms of their antibacterial efficacy. Ag_2O, constituting a predominant phase in the synthesized Ag incorporated hydrogel (as revealed through XRD analysis), plays a major role in contributing to biomedical applications of nanoparticles, including antibacterial and biocompatibility properties. The Ag_2O, along with AgO, releases silver ions (Ag^{+}) in aqueous environments, which have potent antimicrobial properties. These ions penetrate bacterial cells and disrupt essential cellular functions such as enzyme activity, protein synthesis, and DNA replication, leading to cell death [49]. Further, Ag_2O also actively forms reactive oxygen species (ROS) that can cause oxidative stress in bacterial cells, damaging cellular components like lipids, proteins, and nucleic acids, ultimately leading to bacterial death [50].

Therefore, the synthesized hydrogels could be effectively utilized in the pharmaceutical industry to develop wound-healing ointments [33]. The promising antibacterial properties of the hydrogel make it a potential candidate for further exploration in therapeutic and cosmetic applications on a larger scale.

The MTT assay revealed the excellent cytocompatibility of the BSA and BSA-Ag hydrogels. The observed viability of the HEK-293 cells over the incubation period of 48 and 96 h is shown in figure 6(B), highlighting their suitability for biological applications. The bare BSA hydrogel exhibited 96.52% cell viability at 48 h of incubation, which increased to 98.74% at the incubation period of 96 h. Similarly, the BSA5 showed cell viability of 93.24% and 95.62% for 48 h and 96 h incubation, respectively. A comparable increment pattern was observed for the BSA10, with the cell viability rising from 90.76% for 48 h to 93.81% for 96 h. The observed results demonstrate excellent cytocompatibility, indicating the potential of BSA-based hydrogel for biological applications. Mammalian cells possess complex cell membranes and robust antioxidant defense mechanisms, making them less susceptible to Ag+-induced damage at lower concentrations. Also, since Ag_2O is present as the dominant phase in the synthesized Ag-based BSA-hydrogel, the ion release rate is slower in Ag_2O compared to AgNPs, and the latter bears a larger surface area (due to BSA corona), thus possessing a higher reactivity (of AgNps) making it more toxic than Ag_2O [50, 51].

Bai *et al* reported a similar excellent viability of BSA hydrogel with more than a 90% survival rate for L929 cells over 72 h of incubation [52]. Further, no crosslinkers or additives were used to prepare the hydrogel, eliminating any possible toxicity. The AgNPs reportedly can penetrate the human cell membranes and exhibit

cytotoxicity in dose- and concentration-dependent manners. However, entrapment in the hydrogel may help in tuning the release rate of AgNPs to overcome the dose-dependent cytotoxicity while achieving the desired antibacterial functions [53]. Further, the observed reduced cytotoxicity of AgNPs is possibly attributed to their interactions with BSA. Grade *et al* reported the improved cytocompatibility of the AgNPs against the Human gingival fibroblasts (HGFib) cells in the presence of BSA [54]. The enhanced compatibility was attributed to the interactions between BSA and Ag ions, leading to the formation of particle surface coating or binding complexes, reducing toxicity. Bare AgNPs caused complete cell inhibition at the 35 $\mu g\ ml^{-1}$ concentration. In contrast, adding BSA in the solution resulted in only moderate inhibition of HGFib cells, even at a higher concentration of 70 $\mu g\ ml^{-1}$. With excellent cytocompatibility behavior, the synthesized BSA-Ag-composed hydrogels claim their potential for biological applications.

4. Conclusions

This study demonstrates that BSA/AgNP-loaded hydrogels hold a promising potential for biomedical applications, particularly in dermal treatments. A facile *in situ* synthesis procedure was used to form AgNPs with two concentrations of Ag ions, i.e., BSA5 and BSA10 (provided BSA as a matrix protein). The morphological studies obtained through FESEM images and the peaks obtained through the characterization studies, including FTIR and XRD, confirmed the integration of Ag metal ions in the BSA-based hydrogels. Further, the rheological studies revealed that the synthesized hydrogel exhibits excellent elasticity and hydrophilicity, possessing tunable mechanical properties. Additionally, the swelling studies confirmed its capacity to retain water, which is essential for effective dermal application. The synthesized BSA hydrogel integrated with AgNPs also showed excellent antibacterial properties against a broad-spectrum group of pathogenic bacterial strains, which was comparable with the existing antibiotics in the market (i.e., kanamycin). The synthesized hydrogel was found to be biocompatible based on the MTT assay performed on the HEK-293 (mammalian cell line), indicating the cytocompatibility and marking a significant potential of their biological applications. Moreover, while comparing the effect of Ag dosage in the BSA hydrogel samples, BSA10 outperformed BSA5 in terms of higher elastic strength, lower swelling index value, and increased hydrophobiciy. Furthermore, the BSA10 samples showed better antibacterial efficacy against gram-positive and gram-negative pathogenic bacterial strains by possessing almost twice the ZOI compared to BSA5, making them more competent to use against dermal infections. Also, BSA10 possessed improved biocompatibility, promoting cell growth and thereby making them a promising candidate for medical applications. Therefore, this low-cost synthesized hydrogel-NPs system makes it an excellent option to explore for various pharmaceutical industry applications.

Acknowledgments

The Authors are thankful to the Department of Biosciences and Bioengineering and the Indian Institute of Technology Guwahati, India, for providing all necessary instrumentation facilities. The authors also acknowledge the Central Instruments Facility, IIT Guwahati, for providing sophisticated instrumentation facilities. Authors are also obliged to the Ministry of Human Resource Development (MHRD) for TEQIP-III.

Data availability statement

All data that support the findings of this study are included within the article (and any supplementary files).

Declaration of competing interest

The authors declare that they have no known competing financial interests or personal relationships that could have appeared to influence the work reported in this paper.

ORCID iDs

Smrity Sonbhadra https://orcid.org/0000-0001-9071-5592
Rushikesh Fopase https://orcid.org/0000-0001-5715-2257
Anurag Mishra https://orcid.org/0009-0004-9993-8513
Nandini Dhakaan https://orcid.org/0009-0007-8560-9956
Lalit M Pandey https://orcid.org/0000-0002-1664-5730

References

[1] Todros S, Todesco M and Bagno A 2021 Biomaterials and their biomedical applications: from replacement to regeneration *Processes* **9** 1949
[2] Lu L *et al* 2018 The formation mechanism of hydrogels *Curr Stem Cell Res Ther.* **13** 490–6
[3] Shi C X *et al* 2024 Bovine serum albumin-based hydrogels: preparation, properties and biological applications *Chem. Eng. J.* **498** 154651
[4] Zewde B, Atoyebi O, Gugssa A, Gaskell K J and Raghavan D 2021 An investigation of the interaction between bovine serum albumin-conjugated silver nanoparticles and the hydrogel in hydrogel nanocomposites *ACS Omega* **6** 11614–27
[5] Chavez-Esquivel G, Cervantes-Cuevas H, Cortes-Cordova D E, Estrada de los Santos P and Huerta Arcos L 2024 Silver-doped graphite oxide composites used as antimicrobial agents against *Staphylococcus aureus*, *Escherichia coli* and Tatumella terrea evaluated by direct TLC bioautography *Nano Express* **5** 015013
[6] Moreno Ruiz Y P, de Almeida Campos L A, Alves Agreles M A, Galembeck A and Macario Ferro Cavalcanti I 2023 Advanced hydrogels combined with silver and gold nanoparticles against antimicrobial resistance *Antibiotics (Basel)* **12** 104
[7] Chen W, Xie H, Jiang N, Guo X and Liu Z 2023 Synthesis of magnetic sodium lignosulfonate hydrogel(Fe(3)O(4)@LS) and its adsorption behavior for Cd(2+) in wastewater *Int. J. Biol. Macromol.* **245** 125498
[8] Markus J *et al* 2017 Biosynthesis, characterization, and bioactivities evaluation of silver and gold nanoparticles mediated by the roots of chinese herbal angelica pubescens maxim *Nanoscale Res. Lett.* **12** 46
[9] de Camargo A C *et al* 2017 Phenolic acids and flavonoids of peanut by-products: antioxidant capacity and antimicrobial effects *Food Chem.* **237** 538–44
[10] García-Astrain C *et al* 2015 Biocompatible hydrogel nanocomposite with covalently embedded silver nanoparticles *Biomacromolecules* **16** 1301–10
[11] Zabihi M M, Eghbaliferiz S, Khorashadizadeh M, Mortazavi-Derazkola S and Yousefi M 2024 Green synthesis of non-toxic silver nanoparticles using Bunge extract: optimization, cytotoxicity, and antibacterial activities *Results in Chemistry* **7** 101510
[12] Jiang Y, Krishnan N, Heo J, Fang R H and Zhang L 2020 Nanoparticle–hydrogel superstructures for biomedical applications *J. Controlled Release* **324** 505–21
[13] Wahid F, Zhong C, Wang H S, Hu X H and Chu L Q 2017 Recent advances in antimicrobial hydrogels containing metal ions and metals/metal oxide nanoparticles *Polymers (Basel)* **9** 636
[14] Crisan C M, Mocan T, Manolea M, Lasca L I, Tabaran F A and Mocan L 2021 Review on silver nanoparticles as a novel class of antibacterial solutions *Applied Sciences-Basel* **11** 1120
[15] Abdel-Raouf N, Al-Enazi N M and Ibraheem I B M 2017 Green biosynthesis of gold nanoparticles using and characterization of their antibacterial activity *Arabian J. Chem.* **10** S3029–39
[16] Cheng L *et al* 2020 Injectable polypeptide-protein hydrogels for promoting infected wound healing *Adv. Funct. Mater.* **30** 2001196
[17] Habibi N 2014 Preparation of biocompatible magnetite-carboxymethyl cellulose nanocomposite: characterization of nanocomposite by FTIR, XRD, FESEM and TEM *Spectrochim Acta A Mol. Biomol. Spectrosc.* **131** 55–8
[18] Nitu, Fopase R, Pandey L M, Hazarika K P, Borah J P, Singh R K and Srinivasan A 2024 Enhancement in the induction heating efficacy of sol–gel derived SiO_2–CaO–Na_2O–P_2O_5 bioglass-ceramics by incorporating magnetite nanoparticles *J. Mater. Chem.* B **12** 3494–508
[19] Siddiquee M A *et al* 2020 Green synthesis of silver nanoparticles from delonix regia leaf extracts: *in-vitro* cytotoxicity and interaction studies with bovine serum albumin *Mater. Chem. Phys.* **242** 122493
[20] Saxena V and Pandey L M 2019 Synthesis, characterization and antibacterial activity of aluminum doped zinc oxide *Materials Today-Proceedings* **18** 1388–400
[21] Faramawy A M and El-Sayed H M 2023 Optimization of visible photoluminescence emission from Ni-Zn ferrite thin films *Nano Express* **4** 045007
[22] Maestro A, Guzmán E, Ortega F and Rubio R G 2014 Contact angle of micro- and nanoparticles at fluid interfaces *Current Opinion in Colloid & Interface Science* **19** 355–67
[23] Dasgupta N, Ranjan S, Patra D, Srivastava P, Kumar A and Ramalingam C 2016 Bovine serum albumin interacts with silver nanoparticles with a 'side-on' or 'end on' conformation *Chem. Biol. Interact.* **253** 100–11
[24] Nasalapure A V, Chalannavar R K, Kasai D R, Reddy K R and Raghu A V 2021 Novel polymeric hydrogel composites: synthesis, physicochemical, mechanical and biocompatible properties *Nano Express* **2** 030003
[25] Holder I A and Boyce S T 1994 Agar well diffusion assay testing of bacterial susceptibility to various antimicrobials in concentrations non-toxic for human cells in culture *Burns* **20** 426–9
[26] Behera R R, Hasan A, Sankar M R and Pandey L M 2018 Laser cladding with HA and functionally graded TiO_2-HA precursors on Ti–6Al–4V alloy for enhancing bioactivity and cyto-compatibility *Surf. Coat. Technol.* **352** 420–36
[27] Bubpamala T, Viravaidya-Pasuwat K and Pholpabu P 2020 Injectable poly (ethylene glycol) hydrogels cross-linked by metal–phenolic complex and albumin for controlled drug release *ACS Omega* **5** 19437–45
[28] Zhang F, Yang H, Yang Y Q, Wang H, Li X F and Wu X C 2021 Stretchable and biocompatible bovine serum albumin fibrous films supported silver for accelerated bacteria-infected wound healing *Chem. Eng. J.* **417** 129145
[29] Sreekanth T V, Ravikumar S and Lee Y R 2016 Good use of fruit wastes: eco-friendly synthesis of silver nanoparticles, characterization, BSA protein binding studies *J. Mol. Recognit.* **29** 253–9
[30] Sonbhadra S and Pandey L M 2025 Isolation, identification, and characterization of Bacillus subtilis SMP-2 from panitenga and exploring its potential for biosurfactant production *Food Bioprod. Process.* **149** 144–57
[31] Wang G K, Lu Y F, Hou H M and Liu Y F 2017 Probing the binding behavior and kinetics of silver nanoparticles with bovine serum albumin *RSC Adv.* **7** 9393–401
[32] Spinelli P and Polman A 2012 Prospects of near-field plasmonic absorption enhancement in semiconductor materials using embedded Ag nanoparticles *Opt. Express* **20** A641–54
[33] Gallagher L *et al* 2021 Preparation and antimicrobial properties of alginate and serum albumin/glutaraldehyde hydrogels impregnated with silver(I) ions *Chemistry-Switzerland* **3** 672–86
[34] Murugan D *et al* 2024 A facile approach for growing Ag nano-dendrites employing towards cells monitoring using SERS: a proof-of-concept study *Nano Express* **5** 045004
[35] Panda C, Sharma L G and Pandey L M 2023 Experimental procedures to investigate fibrillation of proteins *MethodsX* **11** 102445
[36] Arabi S H, Aghelnejad B, Schwieger C, Meister A, Kerth A and Hinderberger D 2018 Serum albumin hydrogels in broad pH and temperature ranges: characterization of their self-assembled structures and nanoscopic and macroscopic properties *Biomater. Sci.* **6** 478–92

[37] Sabaa M W, Hanna D H, Abu Elella M H and Mohamed R R 2019 Encapsulation of bovine serum albumin within novel xanthan gum based hydrogel for protein delivery *Mater. Sci. Eng. C: Mater. Biol. Appl.* **94** 1044–55
[38] Padilla Villavicencio M *et al* 2020 Ibuprofen photodegradation by Ag_2O and Ag/Ag_2O composites under simulated visible light irradiation *Catal. Lett.* **150** 2385–99
[39] Miranda-Limachi K E, Rodríguez-Núñez Y and Cajachagua-Castro M 2019 Proceso de atención de enfermería como instrumento del cuidado, significado para estudiantes de último curso *Enfermería Universitaria* **16** 374–89
[40] Waghmare M, Khade B, Chaudhari P and Dongre P 2018 Multiple layer formation of bovine serum albumin on silver nanoparticles revealed by dynamic light scattering and spectroscopic techniques *J. Nanopart. Res.* **20** 1–21
[41] Brkic Ahmed L *et al* 2017 Impact of surface functionalization on the uptake mechanism and toxicity effects of silver nanoparticles in HepG2 cells *Food Chem. Toxicol.* **107** 349–61
[42] Prasad Panthi K, Panda C, Mohan Pandey L, Lal Sharma M and Kumar Joshi M Bio-interfacial insights of nanoparticles integrated plant protein-based films for sustainable food packaging applications *Food Reviews International* 1–33
[43] Alam K, Iqbal M, Hasan A and Al-Maskari N 2020 Rheological characterization of biological hydrogels in aqueous state *Journal of Applied Biotechnology Reports* **7** 171–5
[44] Emami-Karvani Z and Chehrazi P 2012 Antibacterial activity of ZnO nanoparticle on gram-positive and gram-negative bacteria *African Journal of Microbiology Research* **5** 1368–73
[45] Porter G C, Schwass D R, Tompkins G R, Bobbala S K R, Medlicott N J and Meledandri C J 2021 AgNP/alginate nanocomposite hydrogel for antimicrobial and antibiofilm applications *Carbohydr Polym.* **251** 117017
[46] Tang S and Zheng J 2018 Antibacterial activity of silver nanoparticles: structural effects *Adv. Healthcare Mater.* **7** 1701503
[47] Ramalingam B, Parandhaman T and Das S K 2016 Antibacterial effects of biosynthesized silver nanoparticles on surface ultrastructure and nanomechanical properties of gram-negative bacteria viz. *Escherichia coli* and *Pseudomonas aeruginosa ACS Appl. Mater. Interfaces* **8** 4963–76
[48] Kora A J and Arunachalam J 2011 Assessment of antibacterial activity of silver nanoparticles on *Pseudomonas aeruginosa* and its mechanism of action *World J. Microb. Biot.* **27** 1209–16
[49] Pandey M *et al* 2021 Targeted and enhanced antimicrobial inhibition of mesoporous ZnO–Ag2O/Ag, ZnO–CuO, and ZnO–SnO2 composite nanoparticles *ACS Omega* **6** 31615–31
[50] Sajjad S *et al* 2019 Synergistic evaluation of AgO(2) nanoparticles with ceftriaxone against CTXM and blaSHV genes positive ESBL producing clinical strains of Uro-pathogenic *E. coli IET Nanobiotechnol.* **13** 435–40
[51] Wang C *et al* 2025 siRNA-AGO2 complex inhibits bacterial gene translation: a promising therapeutic strategy for superbug infection *Cell Rep Med.* 101997
[52] Bai Y *et al* 2019 An injectable robust denatured albumin hydrogel formed via double equilibrium reactions *J. Biomater. Sci. Polym. Ed.* **30** 662–78
[53] Dong Q *et al* 2022 Construction of antibacterial nano-silver embedded bioactive hydrogel to repair infectious skin defects *Biomater. Res.* **26** 36
[54] Grade S *et al* 2012 Serum albumin reduces the antibacterial and cytotoxic effects of hydrogel-embedded colloidal silver nanoparticles *RSC Adv.* **2** 7190–6